Research Square

Preprints are preliminary reports that have not undergone peer review.
They should not be considered conclusive, used to inform clinical practice,
or referenced by the media as validated information.

A spline representation of material properties for laminates, with application to classical laminate theory

Joachim Jørgensen Ågotnes

joachim.j.agotnes@uit.no

UiT The Arctic University of Norway

Tanja Emilie Henriksen

UiT The Arctic University of Norway

Research Article

Keywords: Classical laminate theory, CLT, B-splines, Constitutive interpolation, Laminates, Functionally graded materials, FGM

Posted Date: November 18th, 2026

DOI: https://doi.org/10.21203/rs.3.rs-11596362/v1

License: This work is licensed under a Creative Commons Attribution 4.0 International License.
Read Full License

Additional Declarations: No competing interests reported.

A spline representation of material properties for laminates, with application to classical laminate theory

Joachim Jørgensen Ågotnes[1*] and Tanja Emilie Henriksen[1†]

[1*]Department of Computer Science and Computational Engineering, UiT, Lodve Langesgate 2, Narvik, 8514, Nordland, Norway.

*Corresponding author(s). E-mail(s): joachim.j.agotnes@uit.no;
Contributing authors: tanja.e.henriksen@uit.no;
†These authors contributed equally to this work.

Abstract

The presented work proposes a continuous spline-based representation for the material properties through laminates. A continuous representation is useful when material properties vary over a finite region. The spline representation is applied for classical laminate theory (CLT) to calculate the extensional, coupling, and bending stiffness matrices. Within the laminate, adjacent constitutive states are connected through smooth transitions defined by arithmetic interpolation with a cubic polynomial blending function. This produces a continuously differentiable stiffness field with prescribed transition widths. Explicit expressions are derived for the differences between the spline formulation and the corresponding laminate with sharp interfaces, allowing both symmetric and asymmetric transitions. Symmetric transitions preserve extensional stiffness exactly, while coupling and bending stiffness generally differ. On the other hand, asymmetric transitions can modify all three stiffness matrices. The representation recovers the sharp interface description, as seen in CLT, when the transition widths tend to zero. This provides a framework for assessing how assumed stiffness gradients can influence laminate response. The presented representation's transition widths should be based on the material properties, physical limitations, and/or manufacturing process.

Keywords: Classical laminate theory, CLT, B-splines, Constitutive interpolation, Laminates, Functionally graded materials, FGM

1 Introduction

In the conventional laminate description the material properties, such as stiffness is usually assumed to be constant within each layer and to change abruptly at the interfaces. This representation is appropriate when the constituent layers are approximately homogeneous and separated by distinct interfaces. In some materials, however, the mechanical properties may vary over a finite spatial region. Examples include functionally graded materials, graded metal and ceramic structures, bonded interphases, and additively manufactured components in which composition, porosity, deposition conditions, or thermal history vary through the structure. In such cases, an abrupt change between two constant material states may provide only an approximation of the underlying material distribution.

The objective of the present work is to develop a spline representation of spatially varying stiffness, giving a continuous stiffness representation. Neighbouring material states are connected using local cubic blending over finite transition regions. The resulting field separates the description of the material variation from the numerical resolution used for subsequent integration. This provides local control over the location and width of stiffness transitions, while retaining the selected material states outside these regions.

A continuous stiffness representation provides additional flexibility for describing such variations. Spline theory is particularly suitable for this purpose because it permits local control through selected control values, knot locations, and continuity conditions [1–3]. Instead of introducing additional piecewise constant sublayers to approximate a graded region, the stiffness may be represented directly as a continuous field. The material states, the locations of the transitions between them, and the transition widths can then be treated as parameters of the model.

Classical laminate theory (CLT) provides a well-established analytical framework for relating the properties and orientations of individual layers to the effective mechanical response of laminated structures [4–6]. The extensional, coupling, and bending stiffness matrices, commonly denoted by $\mathbf{A}$, $\mathbf{B}$, and $\mathbf{D}$, are obtained by integrating the material stiffness through the laminate thickness [4, 7, 8]. As a result of its simplicity and computational efficiency, CLT remains an important tool for the analysis and preliminary design of layered structures [6]. The same framework can also been applied to layer based additively manufactured materials, where individual deposited layers can be represented by equivalent anisotropic stiffness properties [9, 10].

Classical laminate theory is used to demonstrate the significance of this additional modelling flexibility. The spline field is integrated through the laminate thickness using the conventional zeroth, first, and second thickness moments to obtain $\mathbf{A}$, $\mathbf{B}$, and $\mathbf{D}$. Explicit expressions are derived for the changes in these stiffness matrices when an abrupt interface is replaced by a cubic transition. The formulation is then assessed using conventional laminates and functionally graded material distributions. The spline representation is not intended to replace the piecewise constant description when sharp material interfaces are physically appropriate. Rather, it provides a parametrised framework for cases in which stiffness varies over a finite region or where the influence of such a variation is of interest. CLT serves here as one application through which the mechanical properties of the stiffness field can be quantified.

Building on existing spline representation of spatially varying material properties, this work develops a local constitutive interpolation framework with explicit control over transition locations and widths. The contribution is a construction that connects predescribed stiffness states through finite cubic transitions. With this construction, it is possible to use analytical expressions for the influence on the extensional, coupling, and bending stiffness matrices within classical laminate theory. These expressions accommodate both symmetric and asymmetric transitions and identify precisely when the corresponding stiffness moments are preserved or modified. In particular, symmetric transitions preserve the extensional stiffness exactly, while generally varying the coupling and bending stiffness.

1.1 Related work

Additively manufactured (AM) parts are constructed layer by layer due to the nature of AM. This process can therefore cause the layers to change the material properties between them due to changes in the AM process. Depending on the manufacturing method, material properties can be affected by local porosity, raster orientation, deposition lines, and variation in thermal history [11–15]. The material properties can therefore be difficult to determine analytically or numerically through the thickness of a laminated structure. Models, such as CLT, can provide a systematic approach for relating these variations at the micro-scale of layered composite laminates [4, 16, 17].

A conventional laminate representation assigns one material state to each modeled layer, disregarding functionally graded materials or regions [18–20]. Therefore, a representation which can describe a smooth transition region within or between plies can be beneficial, e.g.,

$$\mathrm{ply}_k(t) \xrightarrow[\text{transition}]{\text{Smooth}} \mathrm{ply}_{k+1}(t),$$

where each $\mathrm{ply}(t)$ may also be smooth. The material states outside the transition width remain unchanged, while the region between them can be represented independently. This distinction may be useful when material characterization indicates that an interlayer region behaves differently from an ideal sharp interface. The transition width should not, however, be selected only to improve agreement with a measured structural response. For a predictive model, it should instead be related to independent information about the manufactured material or manufacturing process.

A potential method capable of representing layered materials with varying material properties with a transition region or width can be highly beneficial for calculations involving functionally graded materials (FGM). Although transitions between different material properties of FGMs often utilize models such as (1) (see also (42) and [21, 22])

$$P(z) = (P_t - P_b)\left(\frac{z}{h} + \frac{1}{2}\right)^k + P_b, \qquad \text{for } z \in \left[-\frac{h}{2}, \frac{h}{2}\right], \tag{1}$$

where k represents the power, and P_t and P_b represent the material properties at the top and the bottom, respectively, and z is the distance from the reference surface. This method does not, however, consider layered FGM laminates. Spline representations

of spatially varying material properties in multi-material FGMs have been proposed by [23]. Such representations could be incorporated into the present formulation to describe individual graded layers within a laminate. This would allow previously characterized FGMs to be combined with homogeneous or other graded layers, with the resulting laminate response calculated within classical laminate theory.

Bonded interfaces, graded sandwich structures [24], and joining regions provide further use cases for representing layered materials with varying material properties [25]. This type of representation must consider transition widths dependent on how the joining of the materials affects the bonded interfaces [26]. A conventional layered model can already represent a distinct adhesive layer, coating, or core as an additional homogeneous material. This type of varying material representation becomes especially useful when the variations within or around the bonded regions are of interest.

For example, measurements may indicate that stiffness changes gradually between a material and a bonding region. Rather than introducing several artificial sublayers, a small number of material states can be connected by finite transition regions. The transition parameters can then be varied independently to investigate the influence of the local stiffness distribution on the structural response. The same idea can be extended to graded metal and ceramic systems, diffusion-affected regions, and multi-material structures in which neighboring material states are connected through a finite interface. In each case, the spline field provides the material description, while the structural response is determined by the mechanical model in which that field is used.

2 Preliminaries

Classical laminate theory is used in the present work as an application of the stiffness field representation developed in the following section. Standard CLT kinematics, plane stress assumptions, and transformed reduced stiffness notation are adopted throughout [4, 5, 7]. The laminate equations themselves are not modified.

Consider a structure consisting of n material layers with heights $h_k > 0$. The total height and the physical interface locations are

$$h = \sum_{k=1}^{n} h_k, \qquad s_0 = 0, \qquad \text{and} \qquad s_k = \sum_{r=1}^{k} h_r. \tag{2}$$

The coordinate $t \in [0, h]$ is measured from the lower surface, and layer k occupies

$$t \in [s_{k-1}, s_k]. \tag{3}$$

For the laminate calculations, the coordinate measured from the geometric mid plane is

$$z(t) = t - \frac{h}{2}. \tag{4}$$

Each material state is represented by a transformed reduced stiffness matrix $\overline{\mathbf{Q}}_k$. In the conventional laminate description, the through thickness stiffness field is piecewise constant

$$\overline{\mathbf{Q}}_{\mathrm{CLT}}(t) = \overline{\mathbf{Q}}_k, \qquad \text{for } t \in [s_{k-1}, s_k]. \tag{5}$$

The extensional, coupling, and bending stiffness matrices are the zeroth, first, and second moments of the stiffness field

$$\mathbf{A} = \int_0^h \overline{\mathbf{Q}}(t)\, dt, \tag{6}$$

$$\mathbf{B} = \int_0^h z(t)\overline{\mathbf{Q}}(t)\, dt, \tag{7}$$

and

$$\mathbf{D} = \int_0^h z^2(t)\overline{\mathbf{Q}}(t)\, dt, \tag{8}$$

respectively. For $\overline{\mathbf{Q}}(t) = \overline{\mathbf{Q}}_{\mathrm{CLT}}(t)$, these expressions reduce to the standard CLT ply summations. The formulation developed in the following section changes only the through thickness stiffness field $\overline{\mathbf{Q}}(t)$. The definitions of $\mathbf{A}$, $\mathbf{B}$, and $\mathbf{D}$ remain unchanged.

2.1 Spline framework

The piecewise constant field in (5) changes abruptly at each material interface. The proposed representation gives the option for smoothing the transition between sharp material interfaces by implementing a spline framework. The method allows for a finite smoothening width between the interfaces based on the material properties of the constituents. The transition location and its spatial extent therefore become additional parameters.

A 2^{nd} order B-spline curve with blending function (B-function) is constructed by multiplying a basis function, which is generated from a knot vector $\boldsymbol{\tau} = \{\tau_i\}_0^{n+1}$, and control points or local curves [1]. A spline curve is defined as

$$\begin{aligned} c(t) &= \begin{pmatrix} 1 - \mathcal{B} \circ w_{1,i}(t) & \mathcal{B} \circ w_{1,i}(t) \end{pmatrix} \begin{pmatrix} c_{i-1}(t) \\ c_i(t) \end{pmatrix} \\ &= c_{i-1}(t) + \mathcal{B} \circ w_{1,i}(t)\, \Delta c_i(t), \end{aligned} \tag{9}$$

for the knot interval $[\tau_i, \tau_{i+1})$. Where $c(t)$ is the spline curve and where $c_{i-1}(t)$ and $c_i(t)$ are local curves, and $\Delta c_i(t) = c_i(t) - c_{i-1}(t)$. The knot vector for laminate is defined as $\boldsymbol{\tau} = \{\tau_0, \ldots, \tau_{m-1}\}$ where $\{\tau_0, \ldots, \tau_{m-1}\} \in [0, h]$. The B-function $\mathcal{B} \circ w_{1,i}(t)$ blends functions, whether they are based on scalars, matrices, vectors, or point values, and is a simplified notation of

$$\mathcal{B} \circ w_{1,i}(t) = \mathcal{B}(w_{1,i}(t)), \tag{10}$$

where the translation and scaling function is

$$w_{1,i}(t) = \frac{t - \tau_i}{\tau_{i+1} - \tau_i}, \qquad \text{where } \tau_i \leq t < \tau_{i+1}. \tag{11}$$

The B-function $\mathcal{B}(u)$ can vary depending on the desired properties, in the presented work, a cubic polynomial function, $\mathcal{B}(u) = 3u^2 - 2u^3$, was used.

3 Spline representation of stiffness fields

Consider the internal interface s_k between the material states $\overline{\mathbf{Q}}_k$ and $\overline{\mathbf{Q}}_{k+1}$. A general transition region can be defined as

$$I_k = [s_k - a_k, s_k + b_k], \qquad \text{where } a_k, b_k > 0, \tag{12}$$

where a_k and b_k determine the extent of the transition on either side of the interface. The transition regions are required to remain within the two adjacent layers and to have disjoint interiors. We therefore impose

$$0 < a_k \leq h_k, \qquad 0 < b_k \leq h_{k+1}, \qquad \text{for } k = 1, \ldots, n-1,$$

together with

$$b_k + a_{k+1} \leq h_{k+1}, \qquad \text{for } k = 1, \ldots, n-2.$$

Neighbouring transition regions may share an endpoint, where both blends attain the same constitutive state. Within I_k, introduce the normalized local coordinate

$$w_k(t) = \frac{t - (s_k - a_k)}{a_k + b_k}, \qquad \text{where } 0 \leq w_k(t) \leq 1. \tag{13}$$

In this work the B-function used is the cubic polynomial blending function defined as

$$\mathcal{B}(u) = 3u^2 - 2u^3, \qquad \text{for } 0 \leq u \leq 1. \tag{14}$$

The B-functions must satisfy the interpolation conditions

$$\mathcal{B}(0) = 0, \qquad \mathcal{B}(1) = 1, \qquad \text{and where } \mathcal{B}'(0) = \mathcal{B}'(1) = 0. \tag{15}$$

The stiffness field within the transition region is then

$$\overline{\mathbf{Q}}_{\text{spl}}(t) = (1 - \mathcal{B} \circ w_k(t))\, \overline{\mathbf{Q}}_k + \mathcal{B} \circ w_k(t) \overline{\mathbf{Q}}_{k+1}, \qquad \text{for } t \in I_k. \tag{16}$$

On the other hand, outside the transition regions

$$\overline{\mathbf{Q}}_{\text{spl}}(t) = \overline{\mathbf{Q}}_{\text{CLT}}(t). \tag{17}$$

The spline can therefore be represented as

$$\boxed{\overline{\mathbf{Q}}_{\text{spl}}(t) = \begin{cases} (1 - \mathcal{B} \circ w_k(t))\, \overline{\mathbf{Q}}_k + \mathcal{B} \circ w_k(t) \overline{\mathbf{Q}}_{k+1}, & \text{for } t \in I_k \\ \overline{\mathbf{Q}}_{\text{CLT}}(t) & \text{for } t \notin I_k \end{cases}} \tag{18}$$

The conditions in (15) ensure that the transition joins the neighbouring constant regions with a continuous first derivative. For the numerical studies in this work, symmetric transitions are used,

$$a_k = b_k = \delta_k, \tag{19}$$

with

$$\delta_k = \eta \min(h_k, h_{k+1}), \qquad \text{where } 0 < \eta \leq \frac{1}{2}. \tag{20}$$

The relation between the physical layer interfaces and the transition locations is illustrated in Figure 1. For unequal layer heights, the value of δ_k may differ from one interface to the next because it depends on the two neighboring layers.

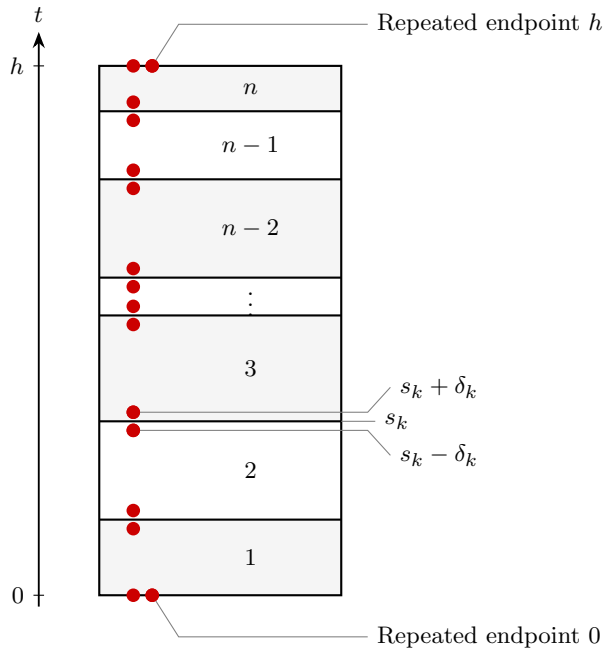


Fig. 1: Schematic knot vector for a layered structure with unequal layer heights. Red points indicate the knot locations used in the spline formulation. Around physical interface s_k, the knots $s_k - \delta_k$ and $s_k + \delta_k$ delimit the local transition interval. The endpoint knots at 0 and h are repeated and shown horizontally separated for visibility.

The red points in Figure 1 represent the knot locations used in the spline formulation. They should be distinguished from the physical interfaces s_k. Each interface defines the nominal location of a material change, while the two neighboring knots $s_k - \delta_k$ and $s_k + \delta_k$ delimit the interval over which the local blending function is active. The knot vector therefore provides the geometric parameterization of the stiffness transitions through the structure.

The corresponding knot vector is constructed from the boundaries of the transition regions,

$$\boldsymbol{\tau} = \big\{0,\, 0,\, s_1 - \delta_1,\, s_1 + \delta_1,\, \ldots,\, s_{n-1} - \delta_{n-1},\, s_{n-1} + \delta_{n-1},\, h,\, h\big\}. \tag{21}$$

The repeated values at 0 and h provide the clamped endpoints used in the numerical implementation. Each pair $s_k - \delta_k$ and $s_k + \delta_k$ defines one local transition interval associated with physical interface s_k. The relation between the physical layer interfaces, the transition regions, and the resulting knot vector is illustrated in Figure 1. For unequal layer heights, δ_k may vary from one interface to the next because it depends on the heights of the two neighbouring layers. The transition region then becomes

$$I_k = [s_k - \delta_k, s_k + \delta_k]. \tag{22}$$

The parameter η controls the spatial extent of the transition. The case $\eta = 0$ is understood as the limiting piecewise constant description. For $\eta \leq 1/2$, neighbouring transition regions do not overlap. Figure 2 illustrates the symmetric construction for one component of the stiffness matrix.

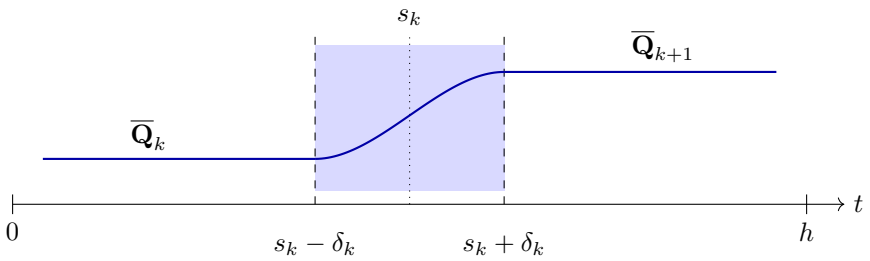


Fig. 2: Schematic representation of one component of the stiffness field around interface s_k. The symmetric transition region has width $2\delta_k$.

3.1 Influence of transition geometry on laminate stiffness

The transition parameters determine how stiffness is redistributed around each interface. Since the laminate stiffness matrices are different thickness moments of the same field, the influence of this redistribution on $\mathbf{A}$, $\mathbf{B}$, and $\mathbf{D}$ is not identical. Define

$$z_{c,k} = s_k - \frac{h}{2}, \qquad \Delta\overline{\mathbf{Q}}_k = \overline{\mathbf{Q}}_{k+1} - \overline{\mathbf{Q}}_k. \tag{23}$$

The following result gives the changes caused by replacing a sharp interface with the cubic transition defined in (12)–(16).

Proposition 1 (Effect of a cubic stiffness transition)**.** *For interface k, the changes relative to the corresponding piecewise constant field are*

$$\Delta\mathbf{A}_k = \frac{a_k - b_k}{2}\Delta\overline{\mathbf{Q}}_k, \tag{24}$$

$$\Delta\mathbf{B}_k = \left[\frac{z_{c,k}(a_k - b_k)}{2} - \frac{3a_k^2 - 4a_k b_k + 3b_k^2}{20}\right]\Delta\overline{\mathbf{Q}}_k, \tag{25}$$

$$\Delta\mathbf{D}_k = \left[\frac{z_{c,k}^2(a_k - b_k)}{2} - \frac{z_{c,k}(3a_k^2 - 4a_k b_k + 3b_k^2)}{10} + \frac{(a_k - b_k)(2a_k^2 - a_k b_k + 2b_k^2)}{30}\right]\Delta\overline{\mathbf{Q}}_k. \tag{26}$$

For several nonoverlapping transitions, the total changes are

$$\mathbf{A}_{\mathrm{spl}} - \mathbf{A}_{\mathrm{CLT}} = \sum_{k=1}^{n-1}\Delta\mathbf{A}_k, \tag{27}$$

$$\mathbf{B}_{\mathrm{spl}} - \mathbf{B}_{\mathrm{CLT}} = \sum_{k=1}^{n-1}\Delta\mathbf{B}_k, \tag{28}$$

$$\mathbf{D}_{\mathrm{spl}} - \mathbf{D}_{\mathrm{CLT}} = \sum_{k=1}^{n-1}\Delta\mathbf{D}_k. \tag{29}$$

For symmetric transitions with

$$a_k = b_k = \delta_k, \tag{30}$$

these expressions reduce to

$$\mathbf{A}_{\mathrm{spl}} - \mathbf{A}_{\mathrm{CLT}} = \mathbf{0}, \tag{31}$$

$$\mathbf{B}_{\mathrm{spl}} - \mathbf{B}_{\mathrm{CLT}} = -\frac{1}{10}\sum_{k=1}^{n-1}\delta_k^2\Delta\overline{\mathbf{Q}}_k, \tag{32}$$

$$\mathbf{D}_{\mathrm{spl}} - \mathbf{D}_{\mathrm{CLT}} = -\frac{1}{5}\sum_{k=1}^{n-1}z_{c,k}\delta_k^2\Delta\overline{\mathbf{Q}}_k. \tag{33}$$

Proof Consider one interface and abbreviate

$$c = s_k, \qquad a = a_k, \qquad b = b_k, \qquad z_c = z_{c,k}, \qquad \text{and} \qquad \Delta\overline{\mathbf{Q}} = \Delta\overline{\mathbf{Q}}_k.$$

Within $[c-a, c+b]$, the spline and piecewise constant fields both contain the contribution $\overline{\mathbf{Q}}_k$. This part therefore cancels when the two fields are subtracted. In the piecewise constant description, the additional contribution $\Delta\overline{\mathbf{Q}}$ is present only on $[c, c+b]$. Hence,

$$\Delta\mathbf{A}_k = \left[\int_{c-a}^{c+b}\mathcal{B}(w(t))\,dt - b\right]\Delta\overline{\mathbf{Q}},$$

$$\Delta\mathbf{B}_k = \left[\int_{c-a}^{c+b} z(t)\mathcal{B}(w(t))\,dt - \int_c^{c+b} z(t)\,dt\right]\Delta\overline{\mathbf{Q}},$$
$$\Delta\mathbf{D}_k = \left[\int_{c-a}^{c+b} z^2(t)\mathcal{B}(w(t))\,dt - \int_c^{c+b} z^2(t)\,dt\right]\Delta\overline{\mathbf{Q}}.$$

Introduce

$$u = w(t) = \frac{t-(c-a)}{a+b}.$$

Then

$$t = c-a+(a+b)u, \qquad dt = (a+b)\,du, \qquad z(t) = z_c - a + (a+b)u, \qquad z_c = c - \frac{h}{2}.$$

For $\mathcal{B}(u) = 3u^2 - 2u^3$,

$$\int_0^1 \mathcal{B}(u)\,du = \frac{1}{2},$$
$$\int_0^1 u\mathcal{B}(u)\,du = \frac{7}{20},$$
$$\int_0^1 u^2\mathcal{B}(u)\,du = \frac{4}{15}.$$

For the zeroth moment,

$$\begin{aligned}\Delta\mathbf{A}_k &= \left[\frac{a+b}{2} - b\right]\Delta\overline{\mathbf{Q}} \\ &= \frac{a-b}{2}\Delta\overline{\mathbf{Q}},\end{aligned}$$

which proves (24).
For the first moment,

$$\int_{c-a}^{c+b} z(t)\mathcal{B}(w(t))\,dt = (a+b)\left[\frac{z_c-a}{2} + \frac{7(a+b)}{20}\right],$$

while

$$\int_c^{c+b} z(t)\,dt = z_c b + \frac{b^2}{2}.$$

Subtracting gives

$$\Delta\mathbf{B}_k = \left[\frac{z_c(a-b)}{2} - \frac{3a^2-4ab+3b^2}{20}\right]\Delta\overline{\mathbf{Q}},$$

which proves (25).
For the second moment,

$$\begin{aligned}&\int_{c-a}^{c+b} z^2(t)\mathcal{B}(w(t))\,dt \\ &\qquad = (a+b)\left[\frac{(z_c-a)^2}{2} + \frac{7(z_c-a)(a+b)}{10} + \frac{4(a+b)^2}{15}\right].\end{aligned}$$

The corresponding piecewise constant contribution is

$$\int_c^{c+b} z^2(t)\,dt = z_c^2 b + z_c b^2 + \frac{b^3}{3}.$$

Subtracting and collecting terms gives

$$\Delta\mathbf{D}_k = \left[\frac{z_c^2(a-b)}{2} - \frac{z_c(3a^2-4ab+3b^2)}{10} + \frac{(a-b)(2a^2-ab+2b^2)}{30}\right]\Delta\overline{\mathbf{Q}},$$

which proves (26).
Since the spline and piecewise constant fields are identical outside the transition regions, the contributions from several nonoverlapping transitions can be added directly. This gives Eqs. (27)–(29).
Finally, setting

$$a_k = b_k = \delta_k$$

gives

$$\Delta\mathbf{A}_k = \mathbf{0}, \qquad \Delta\mathbf{B}_k = -\frac{\delta_k^2}{10}\Delta\overline{\mathbf{Q}}_k, \qquad \Delta\mathbf{D}_k = -\frac{z_{c,k}\delta_k^2}{5}\Delta\overline{\mathbf{Q}}_k.$$

Summing the interface contributions gives Eqs. (31)–(33).

□

3.2 Interpretation of the transition parameters

The formulation separates the stiffness levels from the geometry of the transitions between them. The matrices $\overline{\mathbf{Q}}_k$ determine the material states, the locations s_k determine where changes occur, and the parameters a_k and b_k determine how the transition is distributed around each interface. For a symmetric transition, increasing δ_k redistributes stiffness locally without changing its zeroth thickness moment. Consequently, $\mathbf{A}$ is preserved exactly. The first and second moments may still change because the redistributed stiffness occupies different positions relative to the geometric mid plane. These changes appear through $\mathbf{B}$ and $\mathbf{D}$. For an asymmetric transition with $a_k \neq b_k$, the redistribution is no longer balanced around the original interface. The zeroth moment may then change as well, and all three laminate stiffness matrices can be affected.

The transition parameters therefore provide control over the spatial distribution of stiffness independently of the material states themselves. Classical laminate theory provides a convenient application in which the consequences of this additional spatial information can be quantified through the different moments of the stiffness field.

4 Numerical computation

The numerical examples are used to examine how the additional parameters of the spline stiffness field influence the local material description and the resulting laminate stiffness quantities. The analytical relations derived in Proposition 1 provide a

reference for the numerical implementation, while published material data are used to investigate representative graded stiffness distributions. Two functionally graded materials are considered. The first is a multilayer Titanium – Titanium Boride (Ti/TiB) material for which discrete layer properties are available. This example is used to examine how the transition width changes the stiffness distribution between neighbouring material states. The second is Polyethylene Terephthalate (PETG) reinforced with carbon fibre (CF) and Polylactic Acid (PLA) beam with an explicitly defined continuous modulus profile. Since the underlying field is known analytically, this example allows the piecewise constant and spline representations to be compared directly with a continuous reference stiffness scalar field.

4.1 Comparison with published laminate results

A first set of examples is used to examine how the spline stiffness representation influences previously studied laminate configurations. The selected cases include fibre reinforced composites and additively manufactured polymer laminates for which material properties and stacking sequences have been reported in the literature. The purpose of these comparisons is not to revalidate classical laminate theory. Instead, the published laminates provide a common set of configurations for comparing the conventional piecewise constant stiffness field with the spline representation using the same material input data. In each case, the reported layer properties and stacking sequence are retained, while finite transition regions are introduced between neighbouring stiffness states.

Gomez-Suarez and Lárez-Natera [27] investigated fique fibre reinforced composite laminates and compared their experimental response with analytical and numerical models. Three laminates with different stacking sequences are considered here as Tests 1–3.

Casavola et al. [10] investigated the orthotropic mechanical behaviour of fused deposition modelled ABS and PLA components using classical laminate theory. The lamina properties E_1, E_2, G_{12}, and ν_{12} were obtained experimentally and subsequently used to describe multidirectional laminates. The ABS and PLA cases are used here as Tests 4 and 5.

Glud et al. [28] experimentally characterized the elastic properties of a unidirectional glass fibre reinforced epoxy material and used the resulting properties to describe a multidirectional laminate. The laminate considered in their study is used here as Test 6.

Finally, Ågotnes et al. [9] investigated the use of classical laminate theory for predicting the tensile modulus of fused deposition modelled Tough PLA. The lamina properties E_1, E_2, and G_{12} were obtained from specimens with unidirectional raster orientations, while ν_{12} was taken from literature values. The multiangle laminate considered in that study is used here as Test 7.

The material properties and laminate configurations used in the comparison are summarized in Table 1.

For each laminate, the transformed reduced stiffness matrices are calculated from the reported material properties and orientations. The piecewise constant representation retains one stiffness state within each layer, while the spline representation

Table 1: Material properties and laminate configurations used in the published benchmark cases.

Test	E_1 (MPa)	E_2 (MPa)	G_{12} (MPa)	ν_{12}	h_k (mm)	Stacking sequence	n
Test 1	464.10	258.80	237.60	0.37	1.20	$[0, 90, 0]$	3
Test 2	464.10	258.80	237.60	0.37	1.20	$[90, 0, 90]$	3
Test 3	464.10	258.80	237.60	0.37	1.20	$[90, 0, 45]$	3
Test 4	3120	2770	1247	0.33	0.35	$[30, -30, 0, -30, 30]$	5
Test 5	1790	1150	809	0.344	0.35	$[30, -30, 0, -30, 30]$	5
Test 6	44300	12100	3930	0.36	0.54	$[0, -60, 0, 60, 60, 0, -60, 0]$	8
Test 7	988.41	706.44	257.97	0.36	0.10	$[0, 30, -30, 60, -60, 0, 90]_R$	150

introduces the symmetric transition formulation developed in Section 3. The parameter $\eta = 0.5$ is used for the comparisons reported in this subsection because it represents the widest symmetric transition considered in the present parameter range and therefore makes the influence of the transition regions most visible. For symmetric transitions, Proposition 1 predicts that the extensional stiffness matrix is preserved exactly, while the coupling and bending stiffness matrices may change. To illustrate these changes directly before reducing them to scalar measures, Table 2 gives the complete stiffness matrices for Tests 3 and 7. Test 3 provides an example in which the changes in $\mathbf{B}$ and $\mathbf{D}$ are clearly visible, while Test 7 illustrates a case in which the changes are much smaller.

The matrix comparison confirms the analytical result for symmetric transitions, e.g. $\mathbf{A}_{\text{spl}} = \mathbf{A}_{\text{CLT}}$. The matrices $\mathbf{B}$ and $\mathbf{D}$ may nevertheless differ since they depend on the first and second moments of the through thickness stiffness distribution. Therefore, the magnitude of these matrices can vary substantially between the two laminates. To summarize the matrix level differences across all benchmark cases, the Frobenius norm is used. For a matrix $\boldsymbol{M}$,

$$\|\boldsymbol{M}\|_F = \sqrt{\sum_{i,j} M_{ij}^2}. \tag{34}$$

The relative changes in the extensional and bending stiffness matrices are defined as

$$r_{\mathbf{A}} = 100\frac{\|\mathbf{A}_{\text{spl}} - \mathbf{A}_{\text{CLT}}\|_F}{\|\mathbf{A}_{\text{CLT}}\|_F}, \qquad \text{and} \qquad r_{\mathbf{D}} = 100\frac{\|\mathbf{D}_{\text{spl}} - \mathbf{D}_{\text{CLT}}\|_F}{\|\mathbf{D}_{\text{CLT}}\|_F}. \tag{35}$$

The coupling matrix requires a different normalization because $\mathbf{B}_{\text{CLT}}$ may vanish or have a very small norm. Its change is therefore measured relative to the extensional and bending stiffness scales,

$$r_{\mathbf{B}} = 100\frac{\|\mathbf{B}_{\text{spl}} - \mathbf{B}_{\text{CLT}}\|_F}{\sqrt{\|\mathbf{A}_{\text{CLT}}\|_F \, \|\mathbf{D}_{\text{CLT}}\|_F}}. \tag{36}$$

Table 2: Representative matrix level comparison between the spline and piecewise constant laminate descriptions for Tests 3 and 7 at $\eta = 0.5$. The difference is defined as $\Delta\mathbf{M} = \mathbf{M}_{\text{spl}} - \mathbf{M}_{\text{CLT}}$, where $\mathbf{M} \in \{\mathbf{A}, \mathbf{B}, \mathbf{D}\}$. The units of $\mathbf{A}$, $\mathbf{B}$, and $\mathbf{D}$ are MPa mm, MPa mm^2, and MPa mm^3, respectively.

Matrix	$\mathbf{M}_{\text{spl}}$	$\mathbf{M}_{\text{CLT}}$	$\Delta\mathbf{M}$
	Test 3		
A	$\begin{bmatrix} 1521.294 & 260.685 & 66.680 \\ 260.685 & 1521.294 & 66.680 \\ 66.680 & 66.680 & 742.832 \end{bmatrix}$	$\begin{bmatrix} 1521.294 & 260.685 & 66.680 \\ 260.685 & 1521.294 & 66.680 \\ 66.680 & 66.680 & 742.832 \end{bmatrix}$	$\begin{bmatrix} 0.000 & 0.000 & 0.000 \\ 0.000 & 0.000 & 0.000 \\ 0.000 & 0.000 & 0.000 \end{bmatrix}$
B	$\begin{bmatrix} 287.690 & -131.658 & 78.016 \\ -131.658 & -24.375 & 78.016 \\ 78.016 & 78.016 & -131.658 \end{bmatrix}$	$\begin{bmatrix} 295.066 & -135.033 & 80.017 \\ -135.033 & -25.000 & 80.017 \\ 80.017 & 80.017 & -135.033 \end{bmatrix}$	$\begin{bmatrix} -7.377 & 3.376 & -2.000 \\ 3.376 & 0.625 & -2.000 \\ -2.000 & -2.000 & 3.376 \end{bmatrix}$
D	$\begin{bmatrix} 1515.323 & 231.578 & 101.621 \\ 231.578 & 1870.597 & 101.621 \\ 101.621 & 101.621 & 752.296 \end{bmatrix}$	$\begin{bmatrix} 1504.971 & 227.527 & 104.021 \\ 227.527 & 1889.050 & 104.021 \\ 104.021 & 104.021 & 748.245 \end{bmatrix}$	$\begin{bmatrix} 10.352 & 4.051 & -2.400 \\ 4.051 & -18.454 & -2.400 \\ -2.400 & -2.400 & 4.051 \end{bmatrix}$
	Test 7		
A	$\begin{bmatrix} 13922.246 & 4648.329 & 0.000 \\ 4648.329 & 13207.510 & 0.000 \\ 0.000 & 0.000 & 4313.675 \end{bmatrix}$	$\begin{bmatrix} 13922.246 & 4648.329 & 0.000 \\ 4648.329 & 13207.510 & 0.000 \\ 0.000 & 0.000 & 4313.675 \end{bmatrix}$	$\begin{bmatrix} 0.000 & 0.000 & 0.000 \\ 0.000 & 0.000 & 0.000 \\ 0.000 & 0.000 & 0.000 \end{bmatrix}$
B	$\begin{bmatrix} -6.731 & -10.341 & -29.204 \\ -10.341 & 27.413 & -28.623 \\ -29.204 & -28.623 & -10.341 \end{bmatrix}$	$\begin{bmatrix} -6.763 & -10.328 & -29.229 \\ -10.328 & 27.420 & -28.632 \\ -29.229 & -28.632 & -10.328 \end{bmatrix}$	$\begin{bmatrix} 0.032 & -0.013 & 0.024 \\ -0.013 & -0.007 & 0.009 \\ 0.024 & 0.009 & -0.013 \end{bmatrix}$
D	$\begin{bmatrix} 261901.372 & 87211.493 & -0.198 \\ 87211.493 & 246670.917 & 3.394 \\ -0.198 & 3.394 & 80936.735 \end{bmatrix}$	$\begin{bmatrix} 261902.096 & 87211.465 & -0.563 \\ 87211.465 & 246670.250 & 3.254 \\ -0.563 & 3.254 & 80936.707 \end{bmatrix}$	$\begin{bmatrix} -0.724 & 0.028 & 0.364 \\ 0.028 & 0.667 & 0.140 \\ 0.364 & 0.140 & 0.028 \end{bmatrix}$

The quantities $r_{\mathbf{A}}$, $r_{\mathbf{B}}$, and $r_{\mathbf{D}}$ are dimensionless percentage measures of the changes in the three laminate stiffness matrices. The results for all seven benchmark cases are given in Table 3.

Table 3: Relative changes in the extensional, coupling, and bending stiffness matrices between the spline and piecewise constant representations for $\eta = 0.5$.

Test	$r_{\mathbf{A}}$ (%)	$r_{\mathbf{B}}$ (%)	$r_{\mathbf{D}}$ (%)
Test 1	0.00	0.00	1.10
Test 2	0.00	0.00	1.10
Test 3	0.00	0.42	0.89
Test 4	0.00	0.00	0.10
Test 5	0.00	0.00	0.34
Test 6	0.00	0.00	0.42
Test 7	0.00	0.00	0.00

The results are consistent with the analytical result for symmetric transitions. The extensional stiffness matrix is preserved in every case, giving $r_{\mathbf{A}} = 0$. The influence on the coupling and bending stiffnesses depends on the stacking sequence and on the position of the stiffness changes through the laminate. Among the reported cases, the largest relative change in $\mathbf{D}$ is approximately 1.1%, while Test 3 gives the largest reported change in $\mathbf{B}$ at approximately 0.42%. Test 7 shows much smaller matrix changes. Although these changes are nonzero at the matrix level, as shown in Table 2, they round to approximately zero when reported to two decimal places in the normalized summary.

These benchmark cases demonstrate that a finite transition region can modify the first and second thickness moments while leaving the zeroth moment unchanged. The magnitude of the change depends not only on the difference between neighbouring material states, but also on their location through the laminate. The benchmark calculations should not be interpreted as evidence that a finite transition necessarily improves the predictive accuracy of a laminate model. The published cases are used here to quantify the sensitivity of the laminate stiffness to the additional spatial description introduced by the spline field. A nonzero transition width has a physical interpretation only when such a variation is supported by the material or manufacturing process.

The functionally graded examples considered in the following subsection provide a more direct application of the framework because a spatially varying stiffness field is an inherent feature of those materials.

4.2 Functionally graded stiffness fields

Functionally graded materials or FGMs are composite materials in which the composition, the microstructure, or both vary gradually through the volume of the material so that properties such as stiffness, density, thermal conductivity, or hardness change from one location to another by design. In contrast to conventional composites, where the constituents are distributed uniformly and separated by sharp interfaces, an FGM replaces the abrupt interface with a smooth transition and can reduce the stress concentrations, delamination, and thermal-mismatch problems that sharp interfaces tend to cause. The gradient may take the form of a change in composition, porosity, grain size, or fiber orientation, and it may vary in one, two, or three dimensions. Because different regions of a single component can thereby serve different purposes, FGMs are attractive for applications such as thermal barrier structures, where a heat-resistant ceramic surface grades into a metallic interior. Layer-wise additive manufacturing processes such as FDM are well suited to producing FGMs, since the material, infill, or process parameters can be varied from layer to layer, making the gradient a controllable design variable.

4.2.1 Ti/TiB functionally graded material

Koohbor et al. [29] investigated the through-thickness elastic modulus distribution of a seven-layer Titanium-Titanium Boride (Ti/TiB) functionally graded material. Tensile and four-point bending measurements were combined with an inverse analysis to determine the elastic modulus associated with each layer. The material therefore provides a useful example for studying how a discrete graded stiffness distribution is affected when finite transition regions are introduced between neighbouring material states.

The layer properties used in the present analysis are listed in Table 4. The elastic moduli are taken from [29], while the Poisson's ratios are taken from the related Ti/TiB study [30].

Table 4: Layer properties of the Ti/TiB functionally graded material based on Koohbor et al. [29, 30].

Layer	Ti (vol.%)	TiB (vol.%)	h_k (mm)	E_k (GPa)	ν_k (-)
1	100	0	0.3210	119.13	0.340
2	85	15	0.3200	141.03	0.278
3	70	30	0.4200	188.46	0.238
4	55	45	0.2850	221.25	0.205
5	40	60	0.3810	237.94	0.177
6	25	75	0.3810	316.05	0.152
7	15	85	1.0668	349.97	0.140

For the scalar reduced stiffness used in this example, the value associated with layer k is

$$q_k = \frac{E_k}{1 - \nu_k^2}. \tag{37}$$

The corresponding piecewise constant field is

$$q_{\mathrm{CLT}}(t) = q_k, \qquad \text{where } t \in [s_{k-1}, s_k]. \tag{38}$$

At each internal interface, the transition half-width is obtained from

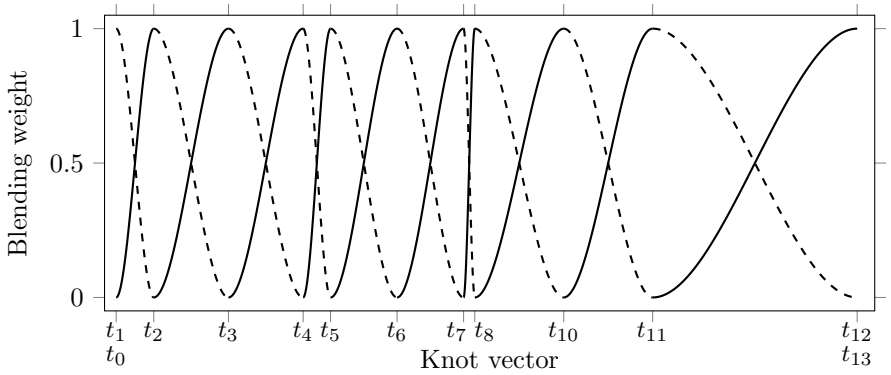
$$\delta_k = \eta \min(h_k, h_{k+1}), \qquad \text{where } 0 \leq \eta \leq \frac{1}{2}. \tag{39}$$

Within the transition region surrounding interface s_k, the spline field is

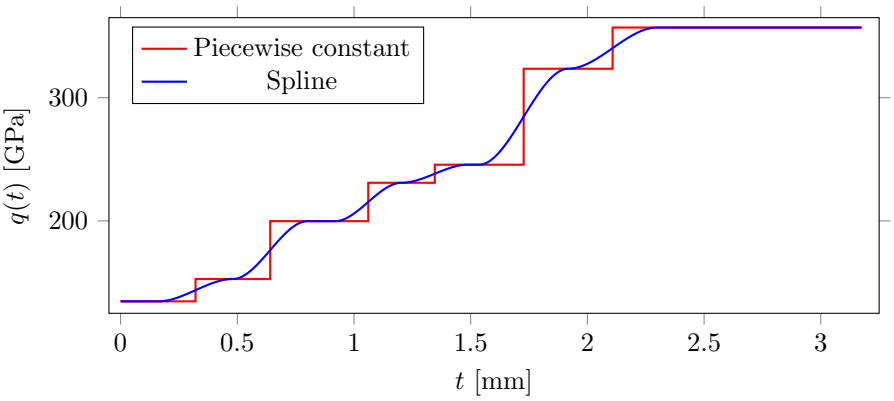
$$q_{\mathrm{spl}}(t) = (1 - \mathcal{B} \circ w_k(t))\, q_k + \mathcal{B} \circ w_k(t) q_{k+1}. \tag{40}$$

Outside the transition regions, the original value q_k is retained. The case $\eta = 0$ therefore corresponds to the original piecewise constant field, while increasing η increases the spatial extent over which neighbouring material states are blended.

The construction for $\eta = 0.5$ is illustrated in Figure 3. The first panel shows the complementary blending weights associated with the knot intervals, while the second shows the resulting through-thickness stiffness field. On intervals where the neighboring stiffness values are equal, the weights may vary without changing $q_{\mathrm{spl}}(t)$. Across a transition between different material states, the same weights produce the smooth variation in stiffness.



(a) Complementary blending weights over the knot vector used for the Ti/TiB stiffness field. The knot locations correspond to the values used in the numerical implementation. The endpoint knots are repeated to obtain the clamped knot vector and are shown at different vertical positions for visibility.



(b) Piecewise constant and spline representations of the through-thickness stiffness field on the physical coordinate t.

Fig. 3: Construction of the Ti/TiB stiffness field for $\eta = 0.5$. The complementary blending weights over the knot intervals are shown in (a), while the resulting stiffness field through the physical laminate height is shown in (b).

The resulting zeroth, first, and second stiffness moments are

$$A = \int_0^h q(t)\,dt, \qquad B = \int_0^h z(t)q(t)\,dt, \qquad D = \int_0^h z^2(t)q(t)\,dt, \tag{41}$$

where $q(t)$ denotes either the piecewise constant or spline field. The influence of η is summarized in Table 5.

The results follow the behaviour predicted by Proposition 1. Since the transitions are symmetric, the zeroth moment of the stiffness field is unchanged and A remains

Table 5: Influence of the transition parameter η on the extensional, coupling, and bending stiffness coefficients of the Ti/TiB stiffness field. The signed differences are calculated relative to the piecewise constant case $\eta = 0$ according to $\Delta X(\eta) = X(\eta) - X(0)$. Unites of **A** , **B** and **D** are [GPa mm], [GPa mm^2], and [GPa mm^3], respectively.

η	A	ΔA	B	ΔB	D	ΔD
0.00	839.5391	0.0000	234.4322	0.0000	681.0402	0.0000
0.05	839.5391	0.0000	234.4255	-0.0067	681.0424	+0.0022
0.10	839.5391	0.0000	234.4056	-0.0266	681.0491	+0.0089
0.20	839.5391	0.0000	234.3260	-0.1062	681.0756	+0.0354
0.50	839.5391	0.0000	233.7684	-0.6638	681.2610	+0.2208

constant for every value of η. Increasing the transition width redistributes stiffness relative to the geometric mid plane and therefore produces changes in B and D. Even for $\eta = 0.5$, the changes in the global stiffness quantities are small. The main effect of η is therefore to control the local distribution of stiffness between neighbouring material states rather than to produce a large change in the overall laminate response. This illustrates an important distinction between the stiffness field itself and its integrated moments.

The Ti/TiB example should not be interpreted as an independent experimental validation of the spline representation. The layer moduli reported by Koohbor et al. were obtained through an inverse identification procedure, and the Poisson's ratios used here are taken from a related study. The example is therefore used primarily to demonstrate the influence of the transition width on a graded set of material states.

4.2.2 PETG/CF and PLA functionally graded beam

Özmen and Özhan [22] investigated functionally graded beams manufactured from Polyethylene Terephthalate (PETG) reinforced with carbon fibre (CF) and Polylactic Acid (PLA). The material composition varied through the beam height according to a power law. This example is particularly useful because the elastic modulus distribution is available as a continuous function. It therefore provides a reference against which the piecewise constant and spline representations can be compared directly. The material properties used in the analysis are given in Table 6.

Table 6: Material properties used for the functionally graded beam investigated by Özmen and Özhan [22].

Material	E (GPa)	ρ (g/cm^3)	ν (-)
PETG/CF	5.74	1.34	0.35
PLA	3.60	1.24	0.27

The power law exponent used by Özmen and Özhan is denoted by p in the present work so that k can be retained as the layer index. With $t \in [0, h]$, the continuous reference field is

$$E_{\mathrm{ref}}(t) = E_{\mathrm{PLA}} + \left(E_{\mathrm{PETG/CF}} - E_{\mathrm{PLA}}\right)\left(\frac{t}{h}\right)^{p}. \tag{42}$$

The beam height is $h = 5$ mm and is divided into 50 layers of equal height,

$$h_k = 0.10 \text{ mm}. \tag{43}$$

The modulus associated with layer k is obtained by evaluating the reference field at the layer midpoint,

$$E_k = E_{\mathrm{ref}}\left(\frac{s_{k-1} + s_k}{2}\right), \qquad \text{for } k = 1, \ldots, 50. \tag{44}$$

The same values E_k are used in the piecewise constant and spline representations. Since all layers have equal height, the transition half width becomes

$$\delta_k = \eta h_k. \tag{45}$$

Within each transition region, the spline field is

$$E_{\mathrm{spl}}(t) = (1 - \mathcal{B} \circ w_k(t))\, E_k + \mathcal{B} \circ w_k(t) E_{k+1}. \tag{46}$$

The case $\eta = 0$ corresponds to the piecewise constant representation. Increasing η increases the spatial extent of the transition between neighbouring values E_k and E_{k+1}.

Since the reference field in (42) is known analytically, its stiffness moments can be evaluated exactly. Define

$$\Delta E = E_{\mathrm{PETG/CF}} - E_{\mathrm{PLA}}. \tag{47}$$

The extensional stiffness is

$$\begin{aligned} A_{\mathrm{ref}} &= \int_0^h \left[E_{\mathrm{PLA}} + \Delta E \left(\frac{t}{h}\right)^{p}\right] dt \\ &= h\left(E_{\mathrm{PLA}} + \frac{\Delta E}{p+1}\right). \end{aligned} \tag{48}$$

The coupling stiffness is

$$\begin{aligned} B_{\mathrm{ref}} &= \int_0^h \left(t - \frac{h}{2}\right)\left[E_{\mathrm{PLA}} + \Delta E \left(\frac{t}{h}\right)^{p}\right] dt \\ &= \frac{\Delta E h^2 p}{2(p+1)(p+2)}. \end{aligned} \tag{49}$$

The bending stiffness is

$$D_{\mathrm{ref}} = \int_0^h \left(t - \frac{h}{2}\right)^2 \left[E_{\mathrm{PLA}} + \Delta E \left(\frac{t}{h}\right)^p\right] dt$$
$$= h^3 \left[\frac{E_{\mathrm{PLA}}}{12} + \frac{\Delta E(p^2+p+2)}{4(p+1)(p+2)(p+3)}\right]. \tag{50}$$

Because the material distribution is generally unsymmetric, extension and bending are coupled. The effective bending stiffness per unit width is therefore evaluated as

$$D^* = D - \frac{B^2}{A}. \tag{51}$$

The quality of the local stiffness representation is measured using the relative L^2 error

$$\varepsilon_E = 100 \sqrt{\frac{\displaystyle\int_0^h \left[E_{\mathrm{model}}(t) - E_{\mathrm{ref}}(t)\right]^2 dt}{\displaystyle\int_0^h E_{\mathrm{ref}}^2(t)\, dt}}. \tag{52}$$

For the global stiffness quantities, signed relative errors are defined as

$$\varepsilon_X = 100 \frac{X_{\mathrm{model}} - X_{\mathrm{ref}}}{X_{\mathrm{ref}}}, \qquad X \in \{A, B, D, D^*\}. \tag{53}$$

The values

$$p = 0.5,\ 1,\ 2,\ 5, \tag{54}$$

are considered together with

$$\eta = 0,\ 0.05,\ 0.10,\ 0.20,\ 0.50. \tag{55}$$

The resulting errors are listed in Table 7.

For every investigated value of p, increasing η reduces the relative L^2 error in the elastic modulus field. The effect is particularly clear for $p = 2$, where ε_E decreases from 0.3272% for the piecewise constant representation to 0.0955% for $\eta = 0.5$. For $p = 1$, the corresponding reduction is from 0.2623% to 0.0723%. The global stiffness quantities are much less sensitive to the transition width. The error in A remains unchanged as η varies, which is consistent with the analytical result for symmetric transitions. The errors in B, D, and D^* are already small for the piecewise constant representation and change only slightly as the transition regions become wider. The results therefore distinguish between two effects of the spline representation. Increasing the transition width can provide a closer description of the underlying continuous stiffness distribution, while the corresponding change in the global stiffness response may remain small. A more accurate local field does not necessarily produce a more accurate value for every thickness moment, since A, B, and D weight the stiffness distribution differently. This behaviour supports the use of the spline representation primarily as a means of introducing additional spatial control into the material description. The

Table 7: Relative errors of the piecewise constant and spline representations with respect to the continuous power law reference field. The case $\eta = 0$ corresponds to the piecewise constant representation. The quantity ε_E denotes the relative L^2 error of the elastic modulus field.

p	η	ε_E (%)	ε_A (%)	ε_B (%)	ε_D (%)	ε_{D^*} (%)
0.5	0.00	0.3151	+0.0070	−0.1590	+0.0237	+0.0271
	0.05	0.2986	+0.0070	−0.1592	+0.0237	+0.0271
	0.10	0.2826	+0.0070	−0.1596	+0.0237	+0.0272
	0.20	0.2523	+0.0070	−0.1612	+0.0239	+0.0274
	0.50	0.1861	+0.0070	−0.1724	+0.0249	+0.0287
1	0.00	0.2623	0.0000	−0.0400	0.0000	+0.0014
	0.05	0.2425	0.0000	−0.0401	0.0000	+0.0014
	0.10	0.2227	0.0000	−0.0405	0.0000	+0.0014
	0.20	0.1835	0.0000	−0.0419	0.0000	+0.0015
	0.50	0.0723	0.0000	−0.0518	0.0000	+0.0018
2	0.00	0.3272	−0.0017	−0.0400	−0.0080	−0.0066
	0.05	0.3027	−0.0017	−0.0401	−0.0080	−0.0066
	0.10	0.2784	−0.0017	−0.0405	−0.0081	−0.0066
	0.20	0.2300	−0.0017	−0.0419	−0.0083	−0.0068
	0.50	0.0955	−0.0017	−0.0518	−0.0098	−0.0079
5	0.00	0.5156	−0.0045	−0.0980	−0.0195	−0.0174
	0.05	0.4794	−0.0045	−0.0981	−0.0195	−0.0175
	0.10	0.4435	−0.0045	−0.0986	−0.0196	−0.0176
	0.20	0.3732	−0.0045	−0.1005	−0.0201	−0.0180
	0.50	0.1920	−0.0045	−0.1139	−0.0232	−0.0209

transition parameter η determines how stiffness is distributed between neighbouring material states, while the influence of this distribution on structural response depends on the particular moment of the field being considered.

5 Discussion

The results clarify both the capabilities and the limitations of the proposed spline representation. The principal effect of the formulation is to replace an abrupt change in constitutive stiffness by a transition that acts over a prescribed finite distance. The standard laminate kinematics and force and moment relations remain unchanged. The difference between the classical and spline descriptions therefore arises entirely from the through-thickness distribution of the constitutive stiffness.

Proposition 1 shows that the effect of the transition depends on both its width and its position relative to the laminate midplane. For a symmetric arithmetic transition, the extensional stiffness is preserved exactly,

$$\mathbf{A}_{\mathrm{spl}} = \mathbf{A}_{\mathrm{CLT}},$$

while the coupling and bending stiffnesses may differ. This result is important because it demonstrates that smoothing an interface does not necessarily alter all components of the laminate response. The transition redistributes stiffness spatially without changing its zeroth thickness moment. The first and second moments may nevertheless

change because they depend on the location of the redistributed stiffness relative to the midplane. For asymmetric transitions, the zeroth moment is no longer preserved, and changes in all three laminate stiffness matrices are possible.

The proposed formulation becomes more relevant when there is a physical reason to associate a finite width with the transition between neighbouring constitutive states. Examples include functionally graded materials, diffusion affected interfaces, deposited material transitions, and regions in which composition or porosity changes over a measurable distance. In these cases, the parameter δ_k has a physical interpretation rather than serving only as a numerical smoothing parameter. The separation between the prescribed material field and the numerical integration resolution is then useful because the constitutive profile can be refined independently of the quadrature used to evaluate the laminate stiffness matrices. The transition width is particularly important because it separates the location of a material change from the distance over which that change occurs. In the symmetric formulation introduced in Section 3, this distance is controlled by δ_k. Varying δ_k therefore provides a direct means of studying the sensitivity of a model to the spatial extent of a stiffness transition. Within the CLT application considered in this work, the consequences of this parameter can be identified analytically. For the symmetric cubic blend, changing δ_k preserves the extensional stiffness matrix $\mathbf{A}$, while the coupling and bending stiffness matrices may change because stiffness is redistributed relative to the geometric mid plane. The transition width therefore provides additional modelling flexibility without necessarily changing all global stiffness quantities. The distinction between the conventional piecewise constant representation and the spline field within CLT is summarized in Table 8.

5.1 Functionally graded materials

Functionally graded materials provide a particularly direct application of the spline representation because their properties are intentionally varied through space. The variation may arise from changes in composition, porosity, fibre volume fraction, or particle content [15]. When material properties are available only at a finite number of locations, the corresponding stiffness values can be used as material states in the spline field. Smooth transitions can then connect these states without requiring the physical gradient to be replaced by a large number of artificially thin constant layers. This provides a useful separation between the material description and the numerical integration. Refining the quadrature changes the accuracy with which the field is integrated, but it does not change the field itself. By contrast, approximating a continuous gradient with an increasing number of constant sublayers changes both the material description and the numerical discretization at the same time. The Ti/TiB and PETG/CF and PLA examples considered in Section 4 illustrate this distinction. In the Ti/TiB example, the spline representation introduces finite transitions between a set of discrete material states. In the PETG/CF and PLA example, the same framework is assessed against an analytically known continuous modulus field. These examples show that the transition width can strongly influence the local description of the stiffness field while having a much smaller effect on its integrated stiffness moments.

The Ti/TiB example illustrates this behaviour numerically. Increasing the transition parameter from $\eta = 0$ to $\eta = 0.5$ leaves the extensional stiffness unchanged at

Table 8: Comparison between the conventional piecewise constant representation and the spline stiffness field when used within classical laminate theory.

Aspect	Piecewise constant CLT representation	Spline stiffness field within CLT
Stiffness through the thickness	Constant within each layer	Constant regions connected by smooth finite width transitions
Interfaces	Ideal abrupt changes	Transitions can extend over a finite region
Material inputs	Layer thickness, orientation, and material properties	Same material states together with transition locations and widths
Numerical integration	Closed form layer summation	Analytical or numerical integration of the continuous field
A, **B**, and **D**	Obtained from piecewise constant stiffness states	Obtained from the same thickness moments applied to the spline field
Suitable material description	Distinct approximately homogeneous layers	Layered or graded materials in which stiffness changes over a finite distance
Additional modelling freedom	Changes are introduced by modifying layers or adding sublayers	Transition width and location can be varied independently of the material states
Physical interpretation	Appropriate when sharp interfaces are a reasonable approximation	Appropriate when smooth or finite width changes are supported by the material architecture

839.5391 GPa mm. Over the same interval, the coupling stiffness changes from 234.4322 to 233.7684 GPa mm^2, while the bending stiffness changes from 681.0402 to 681.2610 GPa mm^3. The effect on the global stiffness quantities is therefore relatively small even when relatively wide transitions are introduced. This is consistent with the analytical result since the transition modifies only a limited region surrounding each interface.

The Ti/TiB example should not, however, be interpreted as an independent experimental validation of the spline formulation. The layer moduli reported by Koohbor et al. were obtained from an inverse identification procedure, and the Poisson's ratios used in the present calculations are taken from a related study. The example is therefore most useful for examining how a reported discrete graded material profile changes when the sharp interfaces are replaced by smooth transitions. A more direct assessment of the constitutive representation is provided by the PETG/CF and PLA beam of Özmen and Özhan. In this case, the continuous power law provides a known reference field. The results show that increasing η reduces the relative L^2 error between the discrete material representation and the prescribed continuous modulus field for

every investigated value of p. For example, for $p = 2$ the relative field error decreases from 0.3272% for the piecewise constant representation to 0.0955% for $\eta = 0.5$. For $p = 1$, the corresponding reduction is from 0.2623% to 0.0723%.

The improvement in the local constitutive representation does not lead to a corresponding improvement in every integrated stiffness quantity. The errors in A, B, D, and D^* are already small for the piecewise constant representation because the 5 mm beam is divided into 50 layers. Increasing η therefore changes these global quantities only slightly. In several cases, the error in B or D increases slightly even though the modulus field becomes closer to the continuous reference field. This distinction is important. A smoother and locally more accurate constitutive field does not necessarily produce a more accurate thickness moment for every response quantity. The value of the spline formulation should therefore not be interpreted as a general improvement over classical CLT. When a laminate consists of distinct homogeneous plies separated by sharp interfaces, the piecewise constant representation remains the natural description. Likewise, when a continuously graded material is represented by a very large number of sufficiently thin layers, the global stiffness coefficients may already be accurately approximated. In such cases, the additional spline description may have little influence on the predicted laminate response.

5.2 Possible engineering benefits

The spline representation provides a framework for representing details that may be lost when a varying material is approximated by a collection of constant layers. The resulting stiffness field can subsequently be used within an appropriate structural model. Classical laminate theory provides one such application in the present work, but the representation itself is not restricted to CLT. Some of the main capabilities of the framework are summarized in Table 9. Their engineering value depends on whether the additional spatial information has a physical interpretation or can be supported by experimental or manufacturing data.

Table 9: Capabilities of the spline stiffness representation and the conditions under which they may provide engineering value.

Capability	Engineering benefit	Condition for usefulness
Finite transition width δ_k	Represents a material change that occurs over a finite spatial region rather than at an ideal sharp interface.	The transition width should have a physical interpretation or be estimated from independent material information.
Local material states	Allows the stiffness field to be modified locally without changing the entire material description.	The available material data must contain information beyond a single homogeneous stiffness value.
Transition location	Allows the position of a material change to be represented explicitly.	The location should correspond to the material architecture or manufacturing process.
Independent numerical integration	The integration resolution can be refined without redefining the stiffness field itself.	The material states and transition parameters remain fixed during numerical refinement.
Use with existing structural models	The continuous stiffness field can be supplied to a structural model without changing the underlying material representation.	The assumptions of the selected structural model must remain appropriate.
Alternative transition functions	Different descriptions of the variation between neighboring material states can be investigated.	The chosen transition should be supported by material behavior or independent observations.

5.3 Limitations of the present application

The transition parameter η should not be regarded as a fitting parameter whose value is selected solely to improve agreement with an experimental result. Its value should preferably be obtained from material characterization, manufacturing information, imaging, or an independently validated numerical model. Without such information, variation of η is most appropriately interpreted as a sensitivity study showing how an assumed transition width influences the predicted response. The present formulation also retains the assumptions of classical laminate theory. It assumes linear elastic behaviour, small deformation, perfect bonding, and negligible transverse shear deformation. The spline representation changes the constitutive field but does not introduce an interface damage model, delamination, plasticity, residual stress, or thermal effects. Applications in which these mechanisms dominate require additional constitutive or structural models. The spline representation adds spatial detail to the stiffness field, but it does not remove the assumptions of the structural model in which the field is used.

The main role of the proposed framework is therefore to provide a more flexible representation of spatially varying material stiffness. Its value depends on whether the additional parameters describe meaningful features of the material. The same stiffness field may subsequently be combined with more advanced structural models when the assumptions of classical laminate theory are insufficient.

6 Future research directions

For future research, it would be beneficial to focus on how transition widths and constitutive control values can be determined from independent material data. Numerical reference models can first be used to assess the influence of these parameters on structural response, followed by experimental assessment where suitable data are available. Further developments include thermal strains, residual stresses and the incorporation of the constitutive representation into theories that account for transverse shear deformation.

6.1 Forged multi-material structures

A possible future direction is to extend the constitutive representation to tensor-product spline surfaces or volumes for forged multi-material structures. One example is pattern-welded steel, often referred to as Damascus or Mosaic Damascus steel, in which different steel compositions are stacked, forge-welded, and deformed to produce material bands and bonded interphases. A spatial spline representation could describe constitutive variation both across and along these bands. An initial study could focus on the elastic stiffness field of the final forged structure. The control values would represent homogenized constitutive states of the constituent steels, while transitions would describe graded interphases where supported by material data. Incorporating this field into a finite element model would allow the influence of band geometry and transition width on mechanical response to be investigated.

Modelling the formulation of the constitutive field during forging would require further development beyond the present linear elastic laminate formulation. A coupled thermomechanical model would need to account for finite deformation, plastic or viscoplastic response, temperature-dependent properties and evolving geometry. Contact, diffusion and phase evolution may also be required, depending on the process and research objective. The present framework therefore offers a starting point for representing the final graded structure, while simulation of its formation requires a more extensive process model.

6.2 Alternative constitutive interpolation laws

The arithmetic blend used here is one possible interpolation of neighboring stiffness states. Future studies could investigate alternative matrix means and their relation to generalized power means [31]. For symmetric positive definite matrices $\overline{\mathbf{Q}}_L$ and $\overline{\mathbf{Q}}_R$, let

$$\lambda = \mathcal{B} \circ w_k(t) \in [0, 1].$$

Three possible interpolation laws are

$$\overline{\mathbf{Q}}_A(\lambda) = (1-\lambda)\overline{\mathbf{Q}}_L + \lambda\overline{\mathbf{Q}}_R, \tag{56}$$

$$\overline{\mathbf{Q}}_H(\lambda) = \left((1-\lambda)\overline{\mathbf{Q}}_L^{-1} + \lambda\overline{\mathbf{Q}}_R^{-1}\right)^{-1}, \tag{57}$$

$$\overline{\mathbf{Q}}_G(\lambda) = \overline{\mathbf{Q}}_L^{1/2}\left(\overline{\mathbf{Q}}_L^{-1/2}\overline{\mathbf{Q}}_R\overline{\mathbf{Q}}_L^{-1/2}\right)^{\lambda}\overline{\mathbf{Q}}_L^{1/2}. \tag{58}$$

These laws preserve positive definiteness, but their physical suitability must be assessed for the material region being represented. Mathematical ordering alone does not establish improved predictive accuracy. Geometric and harmonic interpolation should be applied to the constitutive matrices rather than their individual entries, which may be negative or vanish. The stiffness corrections in Proposition 1 apply to the arithmetic cubic blend. Corresponding expressions or numerical assessments would be needed for the alternative laws.

6.3 Welded plates and heat-affected zones

Welded plates provide another application when the affected region can be represented by a constitutive variation through the thickness. A future study could investigate whether measured stiffness profiles support a direct transition between the parent materials or require an additional constitutive state associated with the weld or heat-affected zone. A possible profile is

$$\overline{\mathbf{Q}}_L \longrightarrow \overline{\mathbf{Q}}_{\mathrm{HAZ}} \longrightarrow \overline{\mathbf{Q}}_R,$$

as illustrated in Figure 4. The left and right affected widths may differ. The intermediate state need not lie between the parent stiffnesses, since the affected material may be softer or stiffer than either parent material.

For a single direct arithmetic transition, (24), (25) and (26) quantify the influence of asymmetric widths. A profile with an additional constitutive state must instead be integrated according to its prescribed pieces. The interface corrections can be summed only when each transition satisfies the assumptions of the proposition. Such a study would assess the elastic consequences of a prescribed affected region. Predicting residual stresses, weld failure or interfacial separation would require additional thermal, damage or interface models.

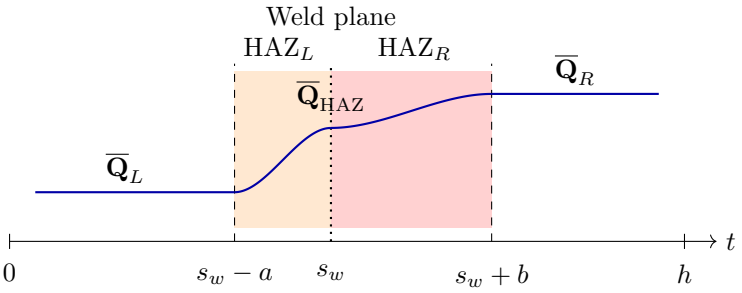


Fig. 4: Illustrative scalar component of a prescribed constitutive field across a welded region with unequal affected widths a and b. The intermediate state and transition shapes require material characterization. The vertical values are schematic and do not imply an ordering of the constitutive matrices.

6.4 Smooth blending preservation

A further research direction is the construction of smooth constitutive transitions that preserve selected laminate stiffness matrices. The symmetric cubic blend preserves $\mathbf{A}$, while other blending functions or transition geometries could be investigated for preserving $\mathbf{B}$ or $\mathbf{D}$. These requirements can be formulated as moment constraints on the difference between the smooth and reference stiffness fields,

$$\int_0^h z(t)^p \big(\overline{\mathbf{Q}}_{\mathrm{spl}}(t) - \overline{\mathbf{Q}}_{\mathrm{CLT}}(t)\big)\, dt = \mathbf{0},$$

where $p = 0, 1, 2$ corresponds to preservation of $\mathbf{A}$, $\mathbf{B}$ and $\mathbf{D}$, respectively. The feasibility of satisfying individual or combined constraints should be examined alongside continuity, positive definiteness and physical admissibility. In particular, preserving both $\mathbf{A}$ and $\mathbf{B}$ across a single non-trivial transition between distinct stiffness states is impossible when the scalar blending weights remain between zero and one. This motivates investigating alternative transition profiles and cancellation of stiffness corrections across multiple interfaces.

7 Conclusion

This paper presents a spline representation of constitutive stiffness within the classical laminate framework. The transformed reduced stiffness is represented as a continuous field through the laminate thickness, with prescribed cubic transitions between adjacent material states. The extensional, coupling and bending stiffness matrices are obtained by integrating this field using the standard laminate moment weights. The formulation therefore retains the existing laminate equations while introducing explicit control over the spatial extent of stiffness transitions.

The principal analytical result is a set of expressions for the changes in laminate stiffness caused by symmetric and asymmetric transitions. For symmetric arithmetic

transitions, the extensional stiffness matrix is preserved exactly, although coupling and bending stiffness generally change. Asymmetric transitions can modify all three stiffness matrices. These results show how transition geometry redistributes stiffness relative to the laminate mid-plane and provide a basis for numerical verification. The corresponding description with sharp interfaces is recovered as the transition widths tend to zero i.e. $\lim_{\delta \to 0}$.

The framework offers a way to represent prescribed material gradients and investigate their influence on laminate response. However, smoothing a stiffness discontinuity does not by itself establish a more accurate material model. The transition widths and constitutive values require physical justification, and the present formulation retains the assumptions and limitations of classical laminate theory.

Further work should compare the formulation with numerical reference solutions for prescribed graded stiffness fields and assess its sensitivity to transition width and interpolation law. Harmonic and geometric interpolation should be investigated through matrix formulations that preserve positive definiteness of the constitutive stiffness. Such comparisons will help determine when the additional modeling flexibility produces a useful improvement over a laminate description with sharp interfaces.

Declarations

Funding

The authors received no specific funding for this work.

Clinical trial registration

Not applicable.

Ethics, Consent to Participate, and Consent to Publish

Ethics, Consent to Participate, and Consent to Publish declarations: not applicable.

Data availability

The material input data used in this study are reported in the cited publications. The numerical results supporting the findings are included in this article.

References

[1] Lakså, A.: Blending Techniques in Curve and Surface Constructions. GEOFO – The Geometry Publishing House, Narvik, Norway (2022). https://www.geofo.no/artikler/BlendBokEng.pdf

[2] Boor, C.: A Practical Guide to Splines. Applied Mathematical Sciences, vol. 27. Springer, Madison, WI, USA (2001). https://doi.org/10.1007/978-1-4612-6333-3

[3] Piegl, L., Tiller, W.: The NURBS Book, 2nd edn. Monographs in Visual Communication. Springer, Berlin, Heidelberg (1997). https://doi.org/10.1007/978-3-642-59223-2

[4] Jones, R.M.: Mechanics of Composite Materials, 2nd edn. CRC press, Boca Raton, FL (2018)

[5] Herakovich, C.: Mechanics of Fibrous Composites - Ebook Edition, New York, NY (2026). https://doi.org/10.5281/zenodo.22178659

[6] Aboudi, J., Arnold, S.M., Bednarcyk, B.A.: Practical Micromechanics of Composite Materials. Butterworth-Heinemann, Oxford, UK (2021)

[7] Öchsner, A.: Advanced Structured Materials Foundations of Classical Laminate Theory vol. 163, 1st edn. Springer, Gewerbestrasse 11, 6330 Cham, Switzerland (2021). https://doi.org/10.1007/978-3-030-82631-4

[8] Haynes, R., Cline, J., Shonkwiler, B., Armanios, E.: On plane stress and plane strain in classical lamination theory. Composites Science and Technology **127** (2016) https://doi.org/10.1016/j.compscitech.2016.02.010

[9] Jørgensen Ågotnes, J., Henriksen, T.E., Entner, E., Beeri Mauseth, G.: Predicting tensile modulus of fused deposition modeled polymer parts using classical laminate theory. Materials & Design **266** (2026) https://doi.org/10.1016/j.matdes.2026.116204

[10] Casavola, C., Cazzato, A., Moramarco, V., Pappalettere, C.: Orthotropic mechanical properties of fused deposition modelling parts described by classical laminate theory. Materials & Design **90** (2016) https://doi.org/10.1016/j.matdes.2015.11.009

[11] Henriksen, T.E., Brustad, T.F., Dalmo, R., Pedersen, A.: Computer-aided optimisation in additive manufacturing processes: A state of the art survey. Journal of Manufacturing and Materials Processing **8** (2024) https://doi.org/10.3390/jmmp8020076

[12] Daly, M., Tarfaoui, M., Chihi, M., Bouraoui, C.: Fdm technology and the effect of printing parameters on the tensile strength of abs parts. International Journal

of Advanced Manufacturing Technology **126**, 5307–5323 (2023) https://doi.org/10.1007/s00170-023-11486-y

[13] Dey, A., Yodo, N.: A systematic survey of fdm process parameter optimization and their influence on part characteristics. Journal of Manufacturing and Materials Processing **3** (2019) https://doi.org/10.3390/jmmp3030064

[14] Santos, N.V., Cardoso, D.C.T.: 3d printing of vegetable yarn-reinforced polymer components. Journal of Cleaner Production **415** (2023) https://doi.org/10.1016/j.jclepro.2023.137870

[15] Reddy, J.N.: Analysis of functionally graded plates. International Journal for Numerical Methods in Engineering **47**(1-3), 663–684 (2000) https://doi.org/10.1002/(SICI)1097-0207(20000110/30)47:1/3⟨663::AID-NME787⟩3.0.CO;2-8

[16] Gibson, R.F.: Principles of Composite Material Mechanics, 2nd edn. CRC Press, Boca Raton, FL (2007). https://doi.org/10.1201/9781420014242

[17] Ahmad, M.N., Ishak, M.R., Yasir, A.S.H.M.: Mechanical, thermal and physical properties of natural fiber reinforced composites for 3d printer - fused deposition modeling: A review. Journal of Materials Research and Technology **39**, 4063–4078 (2025) https://doi.org/10.1016/j.jmrt.2025.10.104

[18] Mohan Sharma, B., Bajpai, T., Kumar Gupta, P., Gautam, V.: Effect of operating parameters of hybrid tig-mig welding on mechanical properties and weld bead quality: A review. Materials Today: Proceedings **118**, 81–86 (2026) https://doi.org/10.1016/j.matpr.2023.01.325 . International Conference on Advanced Research in Industrial & Manufacturing Applications

[19] Bandyopadhyay, A., Heer, B.: Additive manufacturing of multi-material structures. Materials Science and Engineering: R: Reports **129**, 1–16 (2018) https://doi.org/10.1016/j.mser.2018.04.001

[20] Hasanov, S., Gupta, A., Nasirov, A., Fidan, I.: Mechanical characterization of functionally graded materials produced by the fused filament fabrication process. Journal of Manufacturing Processes **58**, 923–935 (2020) https://doi.org/10.1016/j.jmapro.2020.09.011

[21] Jha, D.K., Kant, T., Singh, R.K.: A critical review of recent research on functionally graded plates. Composite Structures **96**, 833–849 (2013) https://doi.org/10.1016/j.compstruct.2012.09.001

[22] Özmen, U., Özhan, B.B.: Mechanics of functionally graded beams: analytical, computational, and experimental analyses. International Journal of Mechanics and Materials in Design **21**(3), 577–590 (2025) https://doi.org/10.1007/s10999-025-09750-y

[23] Wassermann, B., Korshunova, N., Kollmannsberger, S., Rank, E., Elber, G.: Finite cell method for functionally graded materials based on v-models and homogenized microstructures. Advanced Modeling and Simulation in Engineering Sciences **7** (2020) https://doi.org/10.1186/s40323-020-00182-1

[24] Zenkour, A.M.: A comprehensive analysis of functionally graded sandwich plates: Part 1—deflection and stresses. International Journal of Solids and Structures **42**(18), 5224–5242 (2005) https://doi.org/10.1016/j.ijsolstr.2005.02.015

[25] Pietrzak, K., Kaliński, D., Chmielewski, M.: Interlayer of al2o3–cr functionally graded material for reduction of thermal stresses in alumina–heat resisting steel joints. Journal of the European Ceramic Society **27**(2), 1281–1286 (2007) https://doi.org/10.1016/j.jeurceramsoc.2006.04.102 . Refereed Reports IX Conference & Exhibition of the European Ceramic Society

[26] Stein, N., Mardani, H., Becker, W.: An efficient analysis model for functionally graded adhesive single lap joints. International Journal of Adhesion and Adhesives **70**, 117–125 (2016) https://doi.org/10.1016/j.ijadhadh.2016.06.001

[27] Gomez-Suarez, S.A., Lárez-Natera, J.: A multiscale model for tensile response of fique fiber-reinforced composite laminates. AIMS Materials Science **13**(3), 410–443 (2026) https://doi.org/10.3934/matersci.2026021

[28] Glud, J.A., Dulieu-Barton, J.M., Thomsen, O.T., Overgaard, L.C.T.: Fatigue damage evolution in gfrp laminates with constrained off-axis plies. Composites Part A: Applied Science and Manufacturing **95**, 359–369 (2017) https://doi.org/10.1016/j.compositesa.2017.02.005

[29] Koohbor, B., Mallon, S., Kidane, A., Anand, A., Parameswaran, V.: Through thickness elastic profile determination of functionally graded materials. Experimental Mechanics **55**(8), 1427–1440 (2015) https://doi.org/10.1007/s11340-015-0043-z

[30] Koohbor, B., Mallon, S., Kidane, A.: Through thickness fracture behavior of transversely graded ti/tib material. In: Carroll, J., Daly, S. (eds.) Fracture, Fatigue, Failure, and Damage Evolution, Volume 5. Conference Proceedings of the Society for Experimental Mechanics Series, pp. 51–56. Springer, Greenville, SC (2015). https://doi.org/10.1007/978-3-319-06977-7_7

[31] Henriksen, M., Ågotnes, J.J., Persson, L.-E., Samko, S.: Convexity and some new power mean inequalities in continuous forms with illustrations/applications related to heat conduction in composite materials. Mathematical Inequalities & Applications **29**, 353–366 (2026) https://doi.org/10.7153/mia-2026-29-22